Article

Not peer-reviewed version

Simulation of the Catalytic Gasification of Banana Biomass in the Production of Hydrogen, Using Glucose as a Model Compound

Jessica Gaona-Cumbicos , Kelly Naula-Duchi , Paúl Álvarez-Lloret , William Mejía-Galarza , Bolívar Bernal-Pesántez , Lourdes Jara-Cobos *

Posted Date: 9 August 2023

doi: 10.20944/preprints202308.0767.v1

Keywords: simulation, hydrogen, Ansys, Phyton, kinetics.

Article

Simulation of the Catalytic Gasification of Banana Biomass in the Production of Hydrogen, Using Glucose as a Model Compound

Jessica Gaona-Cumbicos [1], Kelly Naula-Duchi [1], Paúl Álvarez-Lloret [1], William Mejía-Galarza [2], Bolívar Bernal-Pesántez [2] and Lourdes Jara-Cobos [1,*]

[1] Reactor Engineering, Catalysis and Environmental Technologies Group, Department of Biosciences, University of Cuenca.; jessica.gaona@ucuenca.edu.ec (J.G-C.); kelly.naula@ucuenca.edu.ec (K.N-D.); paul.alvarez@ucuenca.edu.ec (P.A-LL.); william.mejiag@ucuenca.edu.ec (W.M-G); bolivar.bernal@ucuenca.edu.ec (B.B-P); lourdes.jara@ucuenca.edu.ec (L.J-C.);

[2] Facultad de Ciencias Químicas, Universidad de Cuenca. Cuenca. Ecuador.

* Correspondence: lourdes.jara@ucuenca.edu.ec (L.J-C.);

Abstract: Given the problem of climate change caused by fossil fuels, there is a need to seek efficient alternative energies that have a lower impact on the environment and are obtained from renewable resources. Biomass gasification technology is attracting constant interest in sustainable energy research as an alternative to traditional combustion technology. In gasification, thermochemical conversion of the raw material is carried out, obtaining a gaseous product of great interest known as synthesis gas, gaseous hydrogen, generally used as fuel. Its numerous advantages include the availability of raw materials, reduction in harmful emission streams, performance, and costs. As this is a growing topic within the global energy framework, it is necessary to achieve the maturity of this technology by working on its weaknesses, mainly in terms of efficiency. The objective of this project was to study the hydrogen production process from the simulation of glucose gasification as a biomass model compound through a static model and a dynamic model, in order to determine the maximum concentration of the resulting components in each model studied. Since glucose is the most abundant component in biomass, it was used as a composite model, these models were built, and the basis for the adaptability of subsequent studies of optimization present one was laid. A H_2:CO ratio of 2.2 and molar fluxes were obtained for H_2, CO, CO_2, CH_4 and H_2O as would generally occur in an organic matter gasification process.

Keywords: simulation; hydrogen; Ansys; Phyton; kinetics

1. Introduction

The exponential growth of the world's population and the technological progress essential for survival converge in a common point: the growth of energy demand and the need to supply it [1,2]. This need is closely related to the preservation of regular economic performance [2,3]; therefore, any action on the energy source will have some level of impact [3]. Currently, the focus is on maintaining economic growth strategies, mitigating environmental damage, and improving environmental quality and alternatives against the evident depletion of non-renewable fossil fuel reserves [4]. Environmental quality is affected by the generation of greenhouse gases from using fossil fuels [1,5]. By 2060, the world's oil reserves will be depleted, making it essential to search for sustainable alternatives for energy generation [6]. The main strategy is the production of renewable energies [7].

Renewable Energy is obtained from non-limiting sources and is rapidly acquiring greater interest in applications worldwide [8,9]. Biomass is a potentially significant and ideal source for sustainable energy production [10]. Compared to common conventionally used fuels, biomass has much lower environmental impact and flexibility in its origin, the most common being lignocellulosic residues [11]. Bananas are one of the products with the highest production demand worldwide,

 doi:10.20944/preprints202308.0767.v1

abundant in tropical and subtropical countries [12,13]. As one of the most cultivated plants, it leaves behind large amounts of residues, such as leaves, stems, pseudostems, and fruits, that do not meet quality standards; these residues are used for energy generation [14].

The main components of biomass are lignin, cellulose, and hemicellulose [15]. Cellulose is the compound found in the highest proportion compared to the other components and is composed of repeating units of β-D glucose [16,17]. As cellulose is the main component of biomass and is made up of glucose, glucose becomes the model compound, which, when isolated from biomass, facilitates the process of obtaining energy [18]. Glucose extraction from banana biomass is carried out through different physical, chemical, and biological treatments that simplify operation times and use of resources [17].

One of the approaches to the use of biomass as a renewable energy source is the production of hydrogen, a compound that can be obtained by thermochemical methods that include pyrolysis and liquefaction gasification processes, and by biochemical processes through the use of microorganisms. In addition, thermochemical processes are considered the most optimal for obtaining a hydrogen-rich synthesis gas from biomass [19]. With steam gasification being the most promising for producing hydrogen syngas. In this route, the use of steam as a gasifying agent not only provides Syngas rich in H_2, but also causes minimal environmental impact, especially by avoiding NOx formation with low CO_2 generation, so the hydrogen obtained must be considered "green" [20].

On the other hand, this type of energy is considered as an energy supply for a green and sustainable future, because hydrogen presents ecological, efficient benefits with a great energy potential of approximately 122 MJ/Kg making it an alternative to the use of fossil fuels consumption thanks to its ability to meet the energy demands of the latter. Among the most important advantages of hydrogen are: high energy conversion efficiency, its production with zero water emissions, conversion into fuels, transportation over long distances, etc [21].

The gasification process is one of the most widely used technologies for obtaining renewable Energy from biomass, allowing to get hydrogen, a known energetic vector [22]. Gasification consists of partial thermal oxidation which is produced at a temperature of 800 to 1000 °C in the presence of gasifying agents such as steam or oxygen that provide oxygen to the process [19], the objective of which is to convert biomass into a synthesis gas consisting of carbon dioxide (CO_2), water (H_2O), carbon monoxide (CO), hydrogen (H_2), methane (CH_4), among other gaseous compounds. In addition, small amounts of carbon in solid form, ashes, and other condensable compounds such as tars and oils are produced during the process [22–24]. The proportion of these products in the synthesis gas depends significantly on the biomass composition, raw materials, operating conditions, type of cooker, and gasifying agent [25]. During gasification, cellulose is completely and rapidly converted into glucose at about 400 °C. The main reactions are glucose hydrolysis and water-gas shift [26].

In Table 1 [26] biomass degradation according to its lignocellulosic matter can be observed as a function of temperature, with decomposition starting at temperatures below 373 °C.

Table 1. Biomass decomposition in terms of lignocellulosic matter.

Zone	Temperature Range	Type of Material
I	<373 K	Humidity evolution.
II	373 – 523 K	It takes place at the beginning of the decomposition of hemicellulose.
III	523 – 633 K	Decomposition of cellulose.
IV	633 – 733 K	Lignin decomposition.
V	>733 K	Fixed carbon oxidation.

During the biomass gasification process, two stages are carried out depending on the formation of the products. Stage I involves the formation of char with high concentrations of H_2 and O_2, as well as the cracking of volatile substances. As the temperature rises, the charcoal is transformed into fixed charcoal, which reacts with the gasifying agent to produce synthesis gas in the stage II [22]. The gasification process consists of the following chemical reactions, among them are: drying, thermal

 doi:10.20944/preprints202308.0767.v1

decomposition or pyrolysis, partial combustion of some gases, vapors and charcoal and finally gasification of the decomposition products [19].

Approximately two-thirds of the mass of cellulose is organized into an ordered structure to form stable crystallization zones and high-density hydrogen bonding in crystallization zones makes cellulose less soluble and recalcitrant in conversion. Therefore, cellulose is insoluble in water and in most organic solvents [20].

The gasifier is the vessel where the reactions of the gasification process take place. Its choice will depend on the properties of the biomass, the requirements of the product and the gasifying agent to be used. Among the main ones, three types of gasifiers are used: the upflow and downflow fixed bed gasifier, the fluidized bed gasifier and the entrained flow gasifier. The upflow gasifier has a high thermal efficiency and can handle biomasses with up to 60% moisture; however, they generate more tar. The down-flow gasifier has a low tar production and accepts biomasses with low moisture content of up to 30%. Finally, the fluidized bed has a higher efficiency and biomass conversion due to a more uniform heat distribution [28].

Several studies have come to determine that renewable energy has an indirect effect on attitudes towards the use of renewable energy through the associated impact on the perception of ease of use and perceived usefulness [29]. To optimize processes, biomass must be as cheap as possible, as conditions have a significant impact on cost. Cost estimates are also affected by external factors, such as fluctuating fossil fuel prices, variations in a given country's biofuel policies, and emissions.

According to Adamu & Hossain [23], the kinetic model of the reaction of glucose gasification is described by the Langmuir-Hinshelwood mechanisms, which consists of adsorption processes, desorption during the activation of the reactants, surface reaction, and desorption of the products. In addition, the process is formed by the water-gas shift (WGS) reaction, dry methane reforming reaction (RDRM), and steam methane reforming (SMR) reaction.

The Evolution of this complex reactions scheme can be simulated using specialized software [30], such as Ansys Fluent. This tool allows for studying the fluid's thermal behavior during the glucose gasification process using computational fluid dynamics, showing the temperature distribution in the system [27]. The simulation is framed in three basic stages: a) pre-processing, where the geometric model of the system is defined, followed by the construction of the mesh and the definition of the properties of materials and boundary conditions [31,32], and c) post-processing, where the analyst verifies and validates the model [33].

On the other hand, Python is an open-access programming language useful for scientific computing that can be applied in the chemical area [34,35]. Using material balances for each chemical species and the respective kinetic equations from each reaction generated during the gasification process allows the observation and study of the conversion of the raw material into its products.

In this way, Ansys Fluent will be used to compute the temperature profile inside the chemical reactor where gasification will proceed, and Python will be used to calculate the axial concentration profiles for each chemical species involved in the gasification process.

2. Materials and Methods

Two software, Ansys and Phyton, were used to simulate the gasification process. Ansys CFX was employed for the computational fluid dynamics study. Phyton code was developed to simulate the glucose conversion process into synthesis gas and other derivatives concerning time and the longitudinal axis; that is, a model in a dynamic state and another in a stationary state, respectively.

2.1. Geometry and discretization

The geometry of the whole system is shown in Figure 1, the catalyst-biomass composition is represented by a porous solid of alumina with $\varepsilon = 0.46$ whose measurements are 3 cm internal diameter, 6.6 cm height with inlet and outlet of the fluid through the pipes, whose diameter was 9.25 mm, corresponding to the ¼ inch stainless steel pipes presented as a system in conjunction with the reactor. The porosity corresponding to the catalytic bed was determined by designing the bed with 1 mm spheres packed in a diameter of 3 cm at a height of 10 mm. In both cases, the discretization was

Preprints (www.preprints.org) | NOT PEER-REVIEWED | Posted: 9 August 2023 doi:10.20944/preprints202308.0767.v1

generated in ICEM CDF. In order to obtain a more compact and better quality mesh, the tetrahedron method is used in this refinement, which corresponds to the default set in this module.

The simulation works under manually entered boundary conditions. The internal temperature of the furnace that corresponds to that which has reached a stable state of work, is 639.41 °C, while the gassing agent (water vapor) reached 226.85 °C.

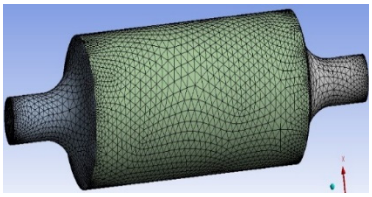

Figure 1. System geometry.

Figure 2 shows the geometry and discretization of the fluid domain (gasifying agent); it is 17 cm long and 9.25 mm in diameter.

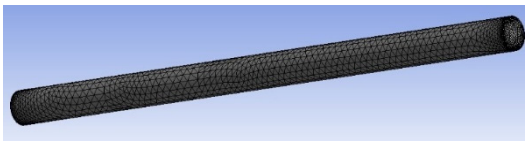

Figure 2. Gassing agent.

2.2. Kinetic model

The mathematical model of the reaction was developed through reaction kinetics using the Langmuir-Hinshelwood mechanism, which involves adsorption of the reactants, catalytic surface reaction, and desorption of the products of the water-gas shift (WGS) reaction, the reverse reaction of dry methane re-forming (RDRM) and the steam reforming reactions of methane (SMR).

2.2.1. Reactions scheme

During the gasification process, the biomass macromolecule is transformed into a series of products, among the main ones are hydrogen H_2, carbon monoxide carbon CO, carbon dioxide CO_2, methane CH_4, water H_2O, and in smaller amounts coke and tars. To represent the gasification process, the following overall reaction is used[36]:

$$C_xH_yO_z + nH_2O \xrightarrow{\Delta} a_1H_2 + a_2CO + a_3CO_2 + a_4H_2O + a_5CH_4 + a_6C + tars \quad (1)$$

Biomass gasification involves a series of chemical reactions through drying, particle decomposition, oxidation, and reduction (WGS, RDRM, and SRM) In equation (1) the amounts of each of the products depend on the operating conditions during the reaction, type of biomass, activity and selectivity of the catalyst. Alumina catalysts are characterized by their high surface area, thermal stability and adsorption capacity, so this stage is the determinant for the reaction kinetics [37].

From the general equation for biomass, we work with a solution of 1.5 mL of glucose at a concentration of 15%, taking as a reference the work done by [20] and the following specific equation:

$$C_6H_{12}O_6 + H_2O \rightarrow CH_4 + 3H_2 + CO_2 + 2H_2O + C \quad (2)$$

Equation (2) represents the process of transformation of glucose to synthesis gas and other components, with this it is possible to determine the number of moles. Once the number of moles and mass of each of the products were obtained, the molar flux was determined considering a reaction time of 25 seconds.

Preprints (www.preprints.org) | NOT PEER-REVIEWED | Posted: 9 August 2023 doi:10.20944/preprints202308.0767.v1

Provided that appropriate assumptions and approximations are established. Therefore, the following assumptions proposed by [21] are made for the kinetic model:

I. Biomass is converted to CO, CO_2, H_2 and CH_4, with traces of coke and tar.

II. The CO, CO_2, H_2, CH_4 and H_2O, are adsorbed on the catalyst surface, which react until they desorb and form part of the product.

III. The dominant reactions in the reaction are water-gas shift (WGS), dry reforming of methane (DRM) and steam reforming of methane (SRM) reactions.

For assumption (I) to be true during the reaction, the reactor pressure should not exceed 57 psi and the main products generated should be CO, CO_2, H_2, CH_4.

In the case of assumption (III), the value of the activation energies of the Bourdouard reaction and methanation must be greater than the SRM, WGS, and reverse dry reforming of methane (RDRM).

Taking these considerations into account, the following equations are presented.

Table 2. Main reactions of the gasification process.

Reaction	Stoichiometry	
The water-gas shift (WGS)	$CO + H_2O \leftrightarrow H_2 + CO_2$	(3)
Steam methane reforming (SMR)	$CH_4 + H_2O \leftrightarrow CO + 3H_2$	(4)
Reverse dry methane reforming (RDRM)	$CH_4 + CO_2 \leftrightarrow 2CO + 2H_2$	(5)

2.2.1. Steam reforming of methane (SRM)

1. Methane adsorption on the active site of the catalyst:

$$CH_4 + S \underset{k2}{\overset{k1}{\rightleftarrows}} CH_4 - S \tag{6}$$

2. Vapor adsorption on the active site of the catalyst:

$$H_2O + S \underset{k4}{\overset{k3}{\rightleftarrows}} H_2O - S \tag{7}$$

3. Surface reaction at the active site of the catalyst:

$$CH_4 - S + H_2O - S + 2S \underset{k6}{\overset{k5}{\rightleftarrows}} CO - S + 3H_2 - S \tag{8}$$

4. CO desorption on the catalyst surface:

$$CO - S + 2S \underset{k8}{\overset{k7}{\rightleftarrows}} CO + S \tag{9}$$

5. Desorption of H_2 from the catalyst surface:

$$H_2 - S \underset{k10}{\overset{k9}{\rightleftarrows}} H_2 + S \tag{10}$$

Considering a pseudo-steady state, the following equation is used to describe the adsorption mechanism [36]

$$r_{SRM} = \frac{k_{SRM} P_{CH_4} P_{H_2O}}{(1 + K_{H_2} P_{H_2} + K_{H_2O} P_{H_2O} + K_{CO} P_{CO} + K_{CO_2} P_{CO_2} + K_{CH_4} P_{CH_4})^4} \times \left(1 - \frac{P_{CO} {P_{H_2}}^3}{K_{SRM} P_{CH_4} P_{H_2O}}\right) \tag{11}$$

where the value of K_{SRM} is the equilibrium rate constant of the SRM, k_{SRM} is the concentrated reaction rate constant for SRM, K_{H_2} is the adsorption rate constant of H_2, K_{H_2O} is the adsorption rate constant of H_2O, K_{CO} is the adsorption rate constant of CO, K_{CO_2} is the adsorption rate constant of CO_2 and K_{CH_4} is the adsorption rate constant of CH_4. P_{H_2} is the pressure of H_2,

Preprints (www.preprints.org) | NOT PEER-REVIEWED | Posted: 9 August 2023 doi:10.20944/preprints202308.0767.v1

P_{H_2O} is the pressure of H_2O, P_{CO} is the pressure of CO , P_{CO_2} is the pressure of CO_2 and P_{CH_4} is the pressure of CH_4.

The equilibrium rate constant is:

$$K_{SRM} = \frac{k_6 K_{CO} {K_{H_2}}^3}{k_5 K_{CH_4} K_{H_2O}} \tag{12}$$

2.2.1.2. The water-gas shift

1. Carbone Monoxide adsorption on the active site of the catalyst:

$$CO + S \underset{k2}{\overset{k1}{\rightleftarrows}} CO - S \tag{13}$$

2. Vapor adsorption on the active site of the catalyst:

$$H_2O + S \underset{k4}{\overset{k3}{\rightleftarrows}} H_2O - S \tag{14}$$

3. Surface reaction at the active site of the catalyst:

$$CO - S + H_2O - S + 2S \underset{k6}{\overset{k5}{\rightleftarrows}} CO_2 - S + H_2 - S \tag{15}$$

4. CO_2 desorption on the catalyst surface:

$$CO_2 - S \underset{k8}{\overset{k7}{\rightleftarrows}} CO_2 + S \tag{16}$$

5. Desorption of H_2 from the catalyst surface:

$$H_2 - S \underset{k10}{\overset{k9}{\rightleftarrows}} H_2 + S \tag{17}$$

Considering a pseudo-steady-state, the following equation is used to describe the adsorption mechanism [36].

$$r_{WGS} = \frac{k_{WGS} P_{CO} P_{H_2O}}{(1 + K_{H_2} P_{H_2} + K_{H_2O} P_{H_2O} + K_{CO} P_{CO} + K_{CO_2} P_{CO_2} + K_{CH_4} P_{CH_4})^2} \times \left(1 - \frac{P_{CO_2} P_{H_2}}{K_{WGS} P_{CO} P_{H_2O}}\right) \tag{18}$$

where the value of K_{WGS} is the equilibrium rate constant of the WGS reaction, k_{WGS} is the concentrated reaction rate constant for WGS, K_{H_2} is the adsorption rate constant of H_2, K_{H_2O} is the adsorption rate constant of H_2O, K_{CO} is the adsorption rate constant of CO, K_{CO_2} is the adsorption rate constant of CO_2 and K_{CH_4} is the adsorption rate constant of CH_4. P_{H_2} is the pressure of H_2, P_{H_2O} is the pressure of H_2O, P_{CO} is the pressure of CO, P_{CO_2} is the pressure of CO_2 and P_{CH_4} is the pressure of CH_4.

The equilibrium rate constant is:

$$K_{WGS} = \frac{k_6 K_{CO_2} K_{H_2}}{k_5 K_{CO} K_{H_2O}} \tag{19}$$

2.2.1.3. Reverse dry methane reforming reaction

1. Carbone Monoxide adsorption on the active site of the catalyst:

$$CO + S \underset{k2}{\overset{k1}{\rightleftarrows}} CO - S \tag{20}$$

2. Vapor adsorption on the active site of the catalyst:

Preprints (www.preprints.org) | NOT PEER-REVIEWED | Posted: 9 August 2023 doi:10.20944/preprints202308.0767.v1

$$H_2 + S \underset{k4}{\overset{k3}{\rightleftarrows}} H_2 - S \quad (21)$$

3. Surface reaction at the active site of the catalyst:

$$2CO\ - S + 2H_2\ - S \underset{k6}{\overset{k5}{\rightleftarrows}} CO_2 - S + CH_4\ - S + 2S \quad (22)$$

4. CO_2 desorption on the catalyst surface:

$$CO_2\ - S \underset{k8}{\overset{k7}{\rightleftarrows}} CO_2 + S \quad (23)$$

5. Desorption of CH_4 from the catalyst surface:

$$CH_4\ - S \underset{k10}{\overset{k9}{\rightleftarrows}} CH_4 + S \quad (24)$$

Considering a pseudo-steady-state, the following equation is used to describe the adsorption mechanism [35].

$$r_{RDRM} = \frac{k_{RDRM} {P_{CO}}^2 {P_{H_2}}^2}{(1+K_{H_2}P_{H_2}+K_{H_2O}P_{H_2O}+K_{CO}P_{CO}+K_{CO_2}P_{CO_2}+K_{CH_4}P_{CH_4})^4} \times \left(1 - \frac{P_{CO_2}P_{CH_4}}{K_{RDRM}{P_{CO}}^2{P_{H_2}}^2}\right) \quad (25)$$

where the value of K_{RDRM} is the equilibrium rate constant for the RDRM reaction, k_{KDRM} is the concentrated reaction rate constant for RDRM, K_{H_2} is the adsorption rate constant of H_2, K_{H_2O} is the adsorption rate constant of H_2O, K_{CO} is the adsorption rate constant of CO, K_{CO_2} is the adsorption rate constant of CO_2 and K_{CH_4} is the adsorption rate constant of CH_4, P_{H_2} is the pressure of H_2, P_{H_2O} is the pressure of H_2O, P_{CO} is the pressure of CO, P_{CO_2} is the pressure of CO_2 and P_{CH_4} is the pressure of CH_4.

The equilibrium rate constant is:

$$K_{RDMR} = \frac{k_5 {K_{CO}}^2 {K_{H_2}}^2}{k_6 K_{CO_2} K_{CH_4}} \quad (26)$$

2.2.2. Reaction rate constants and adsorption rate constant.

The reaction rate constants can be obtained by means of the Arrhenius equation [36].

$$k_j = k_i^0\ exp\left[-\frac{E_a}{RT}\left(\frac{1}{T} - \frac{1}{T_0}\right)\right] \quad (27)$$

And for the adsorption rate constant:

$$K_i = K_i^0\ exp\left[-\frac{\Delta H_i^{ads}}{RT}\left(\frac{1}{T} - \frac{1}{T_0}\right)\right] \quad (28)$$

where k_i corresponds to the adsorption rate constant of component I, k_i^0 corresponds to the pre-exponential factor for component I, ΔH_i^{ads} is the heat of adsorption for component i-th species, T is the reaction temperature and T_0 is the standard Temperature and R is the ideal gas constant.

2.2.3. Dynamic and Steady-State material balance

The additive rate equation was used for component species of the reactions SRM, WGS and RDRM with respect to time [36].

$$R_c = \sum_{j=1}^{Nr} v_{i,j} r_j \quad (29)$$

where $v_{i,j}$ is the stoichiometric coefficient of the t i-th species present in the j-th reaction, for j = 1 to Nr (the number of reactions). Accordingly, the material balance for the dynamic model is as follows:

Preprints (www.preprints.org) | NOT PEER-REVIEWED | Posted: 9 August 2023 doi:10.20944/preprints202308.0767.v1

$$\frac{\forall}{RT}\frac{dP_{H_2}}{dt} = \frac{dn_{H_2}}{dt} = R_{H_2} = (r_{WGS} + 3r_{SRM} - 2r_{RDRM})\, m_{cat} \quad (30)$$

$$\frac{\forall}{RT}\frac{dP_{CO}}{dt} = \frac{dn_{CO}}{dt} = R_{CO} = (-r_{WGS} + r_{SRM} - 2r_{RDRM})\, m_{cat} \quad (31)$$

$$\frac{\forall}{RT}\frac{dP_{CO_2}}{dt} = \frac{dn_{CO_2}}{dt} = R_{CO_2} = (r_{WGS} + r_{RDRM})\, m_{cat} \quad (32)$$

$$\frac{\forall}{RT}\frac{dP_{CH_4}}{dt} = \frac{dn_{CH_4}}{dt} = R_{CH_4} = (-r_{SRM} + r_{RDRM})\, m_{cat} \quad (33)$$

$$\frac{\forall}{RT}\frac{dP_{H_2O}}{dt} = \frac{dn_{H_2O}}{dt} = R_{H_2O} = (-r_{WGS} - r_{RDRM}) * m_{cat} \quad (34)$$

- The steady-state material balance is as follows:

$$\frac{d\dot{n}_{H_2}}{d\forall} = R_{H_2} = (r_{WGS} + 3r_{SRM} - 2r_{RDRM}) \quad (35)$$

$$\frac{d\dot{n}_{CO}}{d\forall} = R_{CO} = (-r_{WGS} + r_{SRM} - 2r_{RDRM}) \quad (36)$$

$$\frac{d\dot{n}_{CO_2}}{d\forall} = R_{CO_2} = (r_{WGS} + r_{RDRM}) \quad (37)$$

$$\frac{d\dot{n}_{CH_4}}{d\forall} = R_{CH_4} = (-r_{SRM} + r_{RDRM}) \quad (38)$$

$$\frac{d\dot{n}_{H_2O}}{d\forall} = R_{H_2O} = (-r_{WGS} - r_{RDRM}) \quad (39)$$

The defined equations of the kinetic models of the main products of the gasification reaction with respect to time and longitudinal axis obtained previously were solved using Python with the indicated parameters in [21] which presents the kinetic parameters used in these equations. In addition, a catalytic mass of 3.92 g, a reactor diameter of 0.03 m was considered.

3. Results and Discussion

3.1. Fluid behavior inside the reactor

3.1.1. Velocity through the reactor

The fluid velocity at the reactor inlet was 0.0065 m/s, but as it crossed the biomass and catalyst bed it showed a decrease, where the most central part has a velocity of about 0.00185 m/s, while at the walls the value tends to zero.

Preprints (www.preprints.org) | NOT PEER-REVIEWED | Posted: 9 August 2023 doi:10.20944/preprints202308.0767.v1

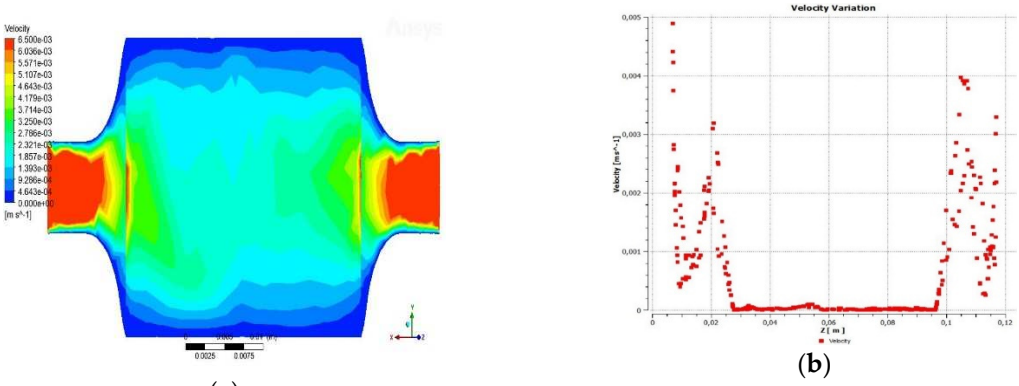

(**a**) (**b**)

Figure 3. a) Behavior of the fluid velocity b) Fluid velocity through the Z-chord.

3.1.2. Temperature across the reactor

The temperature distribution inside the reactor considering the flow of the gasifying agent and the gases generated during the reaction was as follows: the gasifying agent entered the reactor at a temperature of 226.85 °C, while the inner walls of the reactor were at 637.2 °C. Therefore, the fluid as it went through the reactor was acquiring a higher temperature, this being around 604.7 °C, this value was used as the gasification reaction temperature.

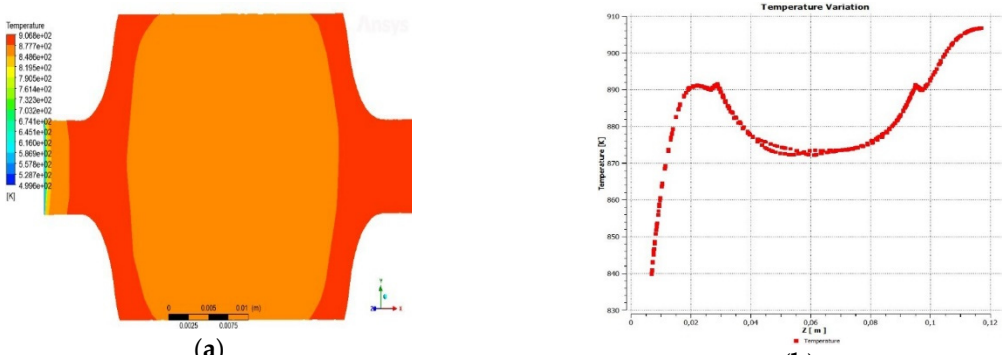

(**a**) (**b**)

Figure 4. a) Fluid temperature distribution b) Temperature variation with respect to Z-axis.

3.1.3. Pressure drop across the reactor

As the fluid passed through the reactor, it presented a resistance, causing a pressure drop, since the steam and gases generated flow through the reactor, so that in the end a negative pressure was obtained, which benefits the exit of the gases by causing them to expand as their density decreases, which facilitates their ascent through the reactor.

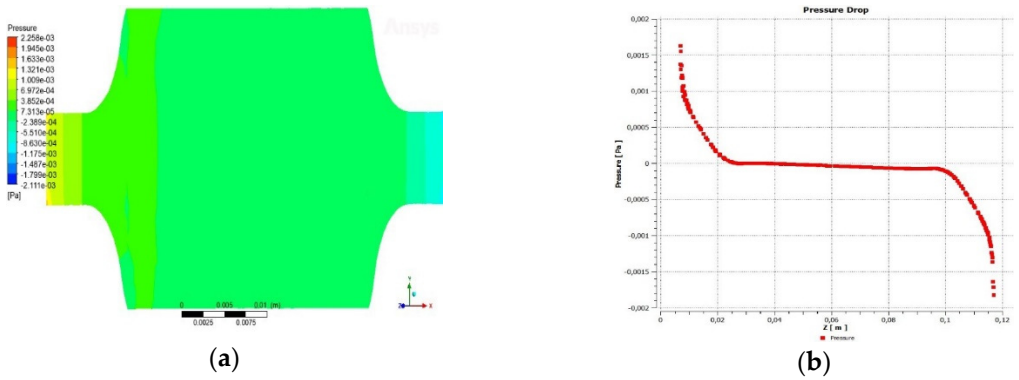

(**a**) (**b**)

Figure 5. a) Pressure variation across the reactor b) Pressure drop with respect to Z-axis.

Preprints (www.preprints.org) | NOT PEER-REVIEWED | Posted: 9 August 2023 doi:10.20944/preprints202308.0767.v1

3.2. Simulation of the gasification reaction

3.2.1. Evolution of the number of moles with respect to time

In the gasification reaction, an increase in the production of carbon dioxide and methane was generated, since they are end products in both the WGS and RDRM reaction, as shown in Figure c and d. The Evolution of the hydrogen yield stabilized at approximately 0.16 mol/s, which according to [38] in his work "Hydrogen production through the gasification of glucose using 5% Ni catalysts with 2% La, Ce and Mg and derivation of an intrinsic reaction rate equation"; he reports resulting values approaching 0.3 mol/s for temperatures close to those above 600 °C and catalysts with higher nickel contents. In addition, [39] in their study "Hydrogen production through glucose gasification using γ-Al2O3 catalysts with Ni, Ce and La and interpretation of results using a non-stoichiometric model", using glucose as biomass model reaches the maximum hydrogen vapor using temperatures up to 600 °C with a reaction time of 30 seconds.

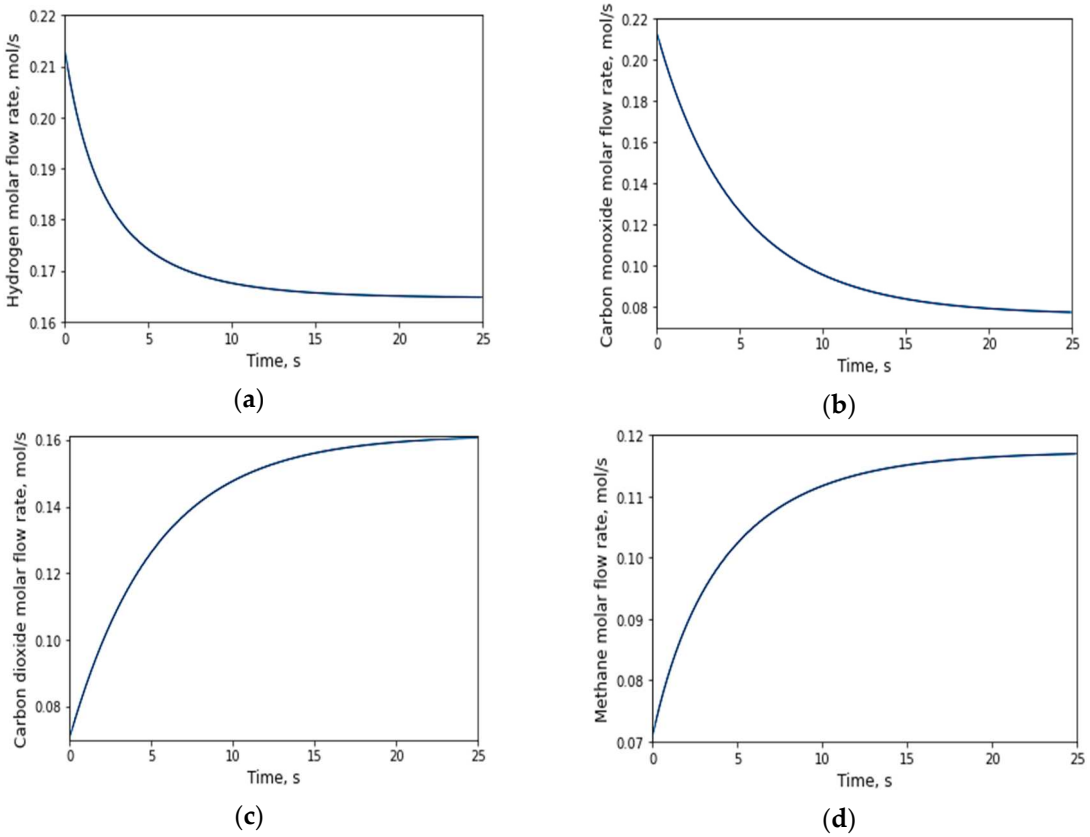

Figure 6. Evolution of the behavior of molar fluxes resulting from the glucose gasification reaction over time. a) Hydrogen flux b) Carbon monoxide flux b) Carbon dioxide flux d) Methane flux.

The constant $H_2{:}CO$ ratio of approximately 2.2. According to [38] in his work "Heterogeneous Catalysis for the Energetic Use of Biomass", he reports values close to or equal to 2 to achieve an optimal use of hydrogen. Generally, a high $H_2{:}CO$ ratio occurs when working at high temperatures, exceeding 500 °C, reaching ranges of between 1.7- 2 [40].

Preprints (www.preprints.org) | NOT PEER-REVIEWED | Posted: 9 August 2023 doi:10.20944/preprints202308.0767.v1

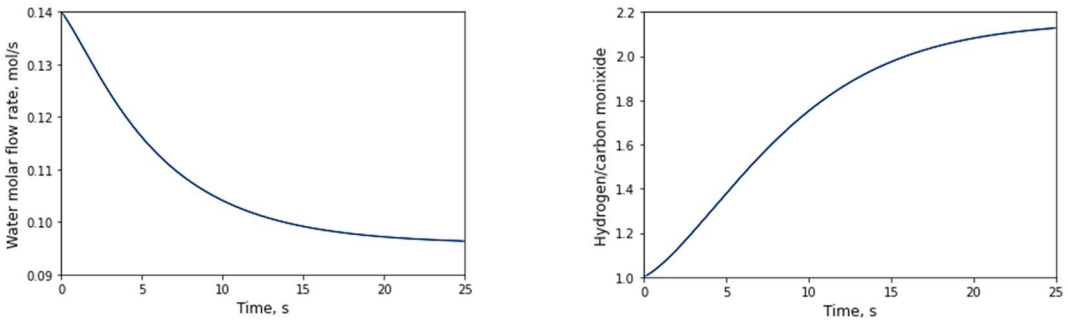

Figure 7. a) Evolution of water flux obtained in the simulation b) Hydrogen/Carbon Monoxide ratio with respect to time.

3.2.1. Evolution of the number of moles with respect to the longitudinal axis

In this case study, the pressure was raised to 2 bar, however, there were no significant changes in obtaining the synthesis gas products compared to the analysis with respect to time. Figure a shows the decrease of hydrogen generated when consumed in the RDRM reaction, this behavior also occurred for figure b, where the trend decreases when consumed in the WGS reaction. For the case of carbon dioxide, an increase was observed, since it is generated only in WGS, this being the predominant reaction. Dry reforming of methane, on the other hand, results in the formation of methane together with carbon dioxide.

In WGS and SRM, one of the reactants is water, this consumption is shown in Figure 8. Finally, the same $H_2{:}CO$ ratio was obtained with the same resultant as in the study with respect to time.

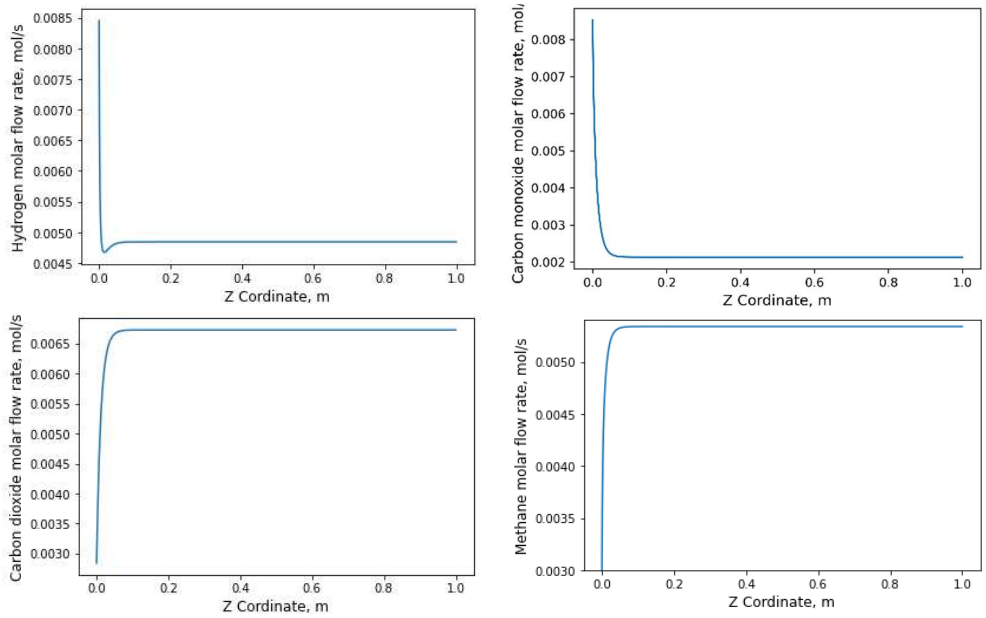

Figure 8. Evolution of flow behavior along the axial z-axis. a) Hydrogen flow b) Carbon monoxide flow c) Carbon dioxide flow d) Methane flow e) Water flow.

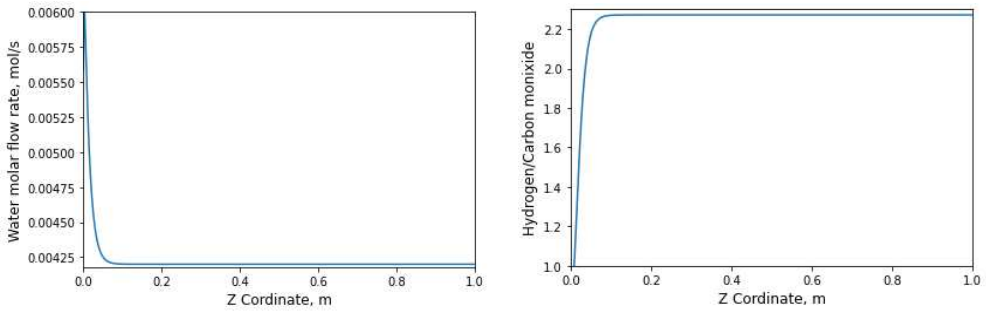

Figure 9. a) Evolution of water flux obtained in the simulation b) Hydrogen/Carbon Monoxide ratio with respect to Z-axis.

4. Conclusion

The glucose gasification process was simulated as a banana biomass model compound, which allowed the study of the behavior of the resulting gases through a kinetic model, based on the Langmuir-Hinshelwood adsorption mechanism. Molar fluxes were obtained for H_2, CO, CO_2, CH_4 and H_2O; presented in behavioral curves for two study cases, the dynamic model and the static model; being so that the results did not present significant variations between the static model and the dynamic model; being so that the results did not present significant variations between the static model and dynamic model. The determining factor, the ratio between hydrogen and carbon monoxide $(H_2:CO)$, showed a value of 2.2, which complied with results presented by other authors in studies of the same type and which means that the process develops as expected and the components obtained are within acceptable values.

A model was presented that, working with real operating conditions, such as temperature, pressure, porosity, molar flow and mass, and adapted to a kinetic model, allowed analyzing the glucose gasification process without the need to invest economic and logistic resources as a physical implementation would, being this the main advantage of the use of software for process simulation and its behaviors. In addition, the work laid the foundations for subsequent studies to be adapted or improved according to each specific case study, which could be optimization studies or economic studies.

Author Contributions: writing—original draft preparation, J.G-C.; and K.N-D.; writing—review and editing, L.J-C.; P.A-LL.; W.M-G. and B.B-P. All authors have read and agreed to the published version of the manuscript.

Funding: This research was funded by VIUC—Universidad de Cuenca.

Conflicts of Interest: The authors declare no conflicts of interest.

References

1. A. G. Olabi and M. A. Abdelkareem, "Renewable energy and climate change," *Renewable and Sustainable Energy Reviews*, vol. 158, p. 112111, Apr. 2022, doi: 10.1016/J.RSER.2022.112111.
2. C.-Y. Feng, X. Yang, S. Afshan, and M. Irfan, "Can renewable energy technology innovation promote mineral resources' green utilization efficiency? Novel insights from regional development inequality," *Resources Policy*, vol. 82, p. 103449, May 2023, doi: 10.1016/J.RESOURPOL.2023.103449.
3. S. Solaymani, E. R. Zada, and A. Gatto, "A Review on Energy and Renewable Energy Policies in Iran," *Sustainability 2021, Vol. 13, Page 7328*, vol. 13, no. 13, p. 7328, Jun. 2021, doi: 10.3390/SU13137328.
4. N. Djellouli, L. Abdelli, M. Elheddad, R. Ahmed, and H. Mahmood, "The effects of non-renewable energy, renewable energy, economic growth, and foreign direct investment on the sustainability of African countries," *Renew Energy*, vol. 183, pp. 676–686, Jan. 2022, doi: 10.1016/J.RENENE.2021.10.066.
5. R. M. Elavarasan *et al.*, "A Comprehensive Review on Renewable Energy Development, Challenges, and Policies of Leading Indian States with an International Perspective," *IEEE Access*, vol. 8, pp. 74432–74457, 2020, doi: 10.1109/ACCESS.2020.2988011.
6. M. Saleem, "Possibility of utilizing agriculture biomass as a renewable and sustainable future energy source," *Heliyon*, vol. 8, no. 2, p. e08905, Feb. 2022, doi: 10.1016/J.HELIYON.2022.E08905.
7. A. Ahmed, T. Ge, J. Peng, W. C. Yan, B. T. Tee, and S. You, "Assessment of the renewable energy generation towards net-zero energy buildings: A review," *Energy Build*, vol. 256, p. 111755, Feb. 2022, doi: 10.1016/J.ENBUILD.2021.111755.
8. L. R. Amjith and B. Bavanish, "A review on biomass and wind as renewable energy for sustainable environment," *Chemosphere*, vol. 293, p. 133579, Apr. 2022, doi: 10.1016/J.CHEMOSPHERE.2022.133579.
9. A. Rahman, O. Farrok, and M. M. Haque, "Environmental impact of renewable energy source based electrical power plants: Solar, wind, hydroelectric, biomass, geothermal, tidal, ocean, and osmotic," *Renewable and Sustainable Energy Reviews*, vol. 161, p. 112279, Jun. 2022, doi: 10.1016/J.RSER.2022.112279.
10. S. Yana, M. Nizar, Irhamni, and D. Mulyati, "Biomass waste as a renewable energy in developing bio-based economies in Indonesia: A review," *Renewable and Sustainable Energy Reviews*, vol. 160, p. 112268, May 2022, doi: 10.1016/J.RSER.2022.112268.

11. Ö. Tezer, N. Karabağ, A. Öngen, C. Ö. Çolpan, and A. Ayol, "Biomass gasification for sustainable energy production: A review," *Int J Hydrogen Energy*, vol. 47, no. 34, pp. 15419–15433, Apr. 2022, doi: 10.1016/J.IJHYDENE.2022.02.158.
12. M. Fiallos-Cárdenas, S. Pérez-Martínez, and A. D. Ramirez, "Prospectives for the development of a circular bioeconomy around the banana value chain," *Sustain Prod Consum*, vol. 30, pp. 541–555, Mar. 2022, doi: 10.1016/J.SPC.2021.12.014.
13. M. Verma and V. Mishra, "Bioelectricity generation by microbial degradation of banana peel waste biomass in a dual-chamber S. cerevisiae-based microbial fuel cell," *Biomass Bioenergy*, vol. 168, p. 106677, Jan. 2023, doi: 10.1016/J.BIOMBIOE.2022.106677.
14. R. K. Singh, T. Patil, D. Pandey, S. P. Tekade, and A. N. Sawarkar, "Co-pyrolysis of petroleum coke and banana leaves biomass: Kinetics, reaction mechanism, and thermodynamic analysis," *J Environ Manage*, vol. 301, p. 113854, Jan. 2022, doi: 10.1016/J.JENVMAN.2021.113854.
15. D. C. Dayton and T. D. Foust, "Analytical methods for biomass characterization and conversion," *Analytical Methods for Biomass Characterization and Conversion*, pp. 1–260, Jan. 2020, doi: 10.1016/C2017-0-03467-5.
16. X. Wang, S. Yang, B. Shen, J. Yang, and L. Xu, "Pyrolysis of Biomass Pineapple Residue and Banana Pseudo-Stem: Kinetics, Mechanism and Valorization of Bio-Char," *Catalysts*, vol. 12, no. 8, p. 840, Aug. 2022, doi: 10.3390/CATAL12080840/S1.
17. P. Subramanian, S. Sriramajayam, P. Vijayakumary, K. Raja, M. Reddy, and P. G. Research, "Extraction of cellulose from banana sheath and its characterization," *~ 1861 ~ The Pharma Innovation Journal*, vol. 11, no. 6, pp. 1861–1867, 2022, Accessed: Apr. 04, 2023. [Online]. Available: www.thepharmajournal.com
18. " Francisco, G. Salinas, P. Obtener, G. De, I. Q. Mario, and A. G. Gallardo, "Producción de hidrógeno a través de la gasificación de glucosa usando catalizadores de 5%Ni con 2% de La, Ce y Mg y deducción de una ecuación de velocidad de reacción intrínseca," 2019, Accessed: Apr. 04, 2023. [Online]. Available: http://ricaxcan.uaz.edu.mx/jspui/handle/20.500.11845/2306
19. L. Jara-Cobos, M. Abril-González, and V. Pinos-Vélez, "Production of Hydrogen from Lignocellulosic Biomass: A Review of Technologies," *Catalysts*, vol. 13, no. 4. MDPI, Apr. 01, 2023. doi: 10.3390/catal13040766.
20. L. Jara-Cobos, M. Abril-González, and V. Pinos-Vélez, "Production of Hydrogen from Lignocellulosic Biomass: A Review of Technologies," *Catalysts*, vol. 13, no. 4, p. 766, Apr. 2023, doi: 10.3390/catal13040766.
21. D. Tacuri *et al.*, "Design and Development of a Catalytic Fixed-Bed Reactor for Gasification of Banana Biomass in Hydrogen Production," *Catalysts*, vol. 12, no. 4, Apr. 2022, doi: 10.3390/catal12040395.
22. J. Yu, Q. Guo, Y. Gong, L. Ding, J. Wang, and G. Yu, "A review of the effects of alkali and alkaline earth metal species on biomass gasification," *Fuel Processing Technology*, vol. 214, no. December 2020, p. 106723, 2021, doi: 10.1016/j.fuproc.2021.106723.
23. S. Adamu and M. M. Hossain, "Kinetics of Steam Gasification of Glucose as a Biomass Surrogate over Ni/Ce-Mesoporous Al2O3 in a Fluidized Bed Reactor," *Ind Eng Chem Res*, vol. 57, no. 9, pp. 3128–3137, Mar. 2018, doi: 10.1021/acs.iecr.7b04437.
24. S. Bhushan, M. S. Rana, Mamta, N. Nandan, and S. K. Prajapati, "Energy harnessing from banana plant wastes: A review," *Bioresource Technology Reports*, vol. 7. Elsevier Ltd, Sep. 01, 2019. doi: 10.1016/j.biteb.2019.100212.
25. Y. Zhang, L. Li, P. Xu, B. Liu, Y. Shuai, and B. Li, "Hydrogen production through biomass gasification in supercritical water: A review from exergy aspect," *Int J Hydrogen Energy*, vol. 44, no. 30, pp. 15727–15736, 2019, doi: 10.1016/j.ijhydene.2019.01.151.
26. M. B. García-Jarana, J. R. Portela, J. Sánchez-Oneto, E. J. M. de la Ossa, and B. Al-Duri, "Analysis of the supercriticalwater gasification of cellulose in a continuous system using short residence times," *Applied Sciences (Switzerland)*, vol. 10, no. 15, Aug. 2020, doi: 10.3390/app10155185.
27. F. R. Flores Guamán, "Determinación de la capacidad calorífica de biomasas residuales de la producción agrícola del Ecuador," Universidad Central de Ecuador, 2022.
28. Y. A. Situmorang, Z. Zhao, A. Yoshida, A. Abudula, and G. Guan, "Small-scale biomass gasification systems for power generation (<200 kW class): A review," *Renewable and Sustainable Energy Reviews*, vol. 117, no. January 2019, p. 109486, 2020, doi: 10.1016/j.rser.2019.109486.
29. [29] T.-Z. Ang, M. Salem, M. Kamarol, H. S. Das, M. A. Nazari, and N. Prabaharan, "A comprehensive study of renewable energy sources: Classifications, challenges and suggestions," Energy Strategy Rev., vol. 43, p. 100939, Sep. 2022, doi: 10.1016/j.esr.2022.100939.
30. S. Zalamea, Mejía William, and J. Serrano, "Kinetic and mathematical modeling of the catalytic supercritical water gasification of the glucose for the hydrogen production," *Revista de la Facultad de Ciencias Químicas*, pp. 1–11, Apr. 2016.
31. F. J. Espinilla Peña, "Elaboración de un modelo 3D de una turbina de vapor," 2019, Accessed: Apr. 06, 2023. [Online]. Available: https://riull.ull.es/xmlui/handle/915/13373
32. J. O. C. Escobar, F. Jurado, and D. Vera, "Simulation of an active indirect hybrid dehydrator using ANSYS software," *Enfoque UTE*, vol. 12, no. 4, pp. 29–44, Oct. 2021, doi: 10.29019/ENFOQUEUTE.771.

33. A. B. Parrilla, "Simulación 2D de la rotura de Presa de Malpasset con los modelos Iber y RiverFlow2D ," 2019.
34. J. Carlos and J. Bedolla, "Métodos numéricos usando Python con aplicaciones a la Ingeniería Química".
35. S. A. Lemus-Contreras, T. B. Pavón-Silva, M. L. H. Alva, and Y. Zarazúa-Aguilar, "Desarrollo de un programa con Python para la determinación de datos cinéticos en reacciones irreversibles de un solo componente en reactores intermitentes," *Journal of Basic Sciences*, vol. 8, no. 23, pp. 11–34, Aug. 2022, doi: 10.19136/JOBS.A8N23.5342.
36. S. Adamu and M. M. Hossain, "Kinetics of Steam Gasification of Glucose as a Biomass Surrogate over Ni/Ce-Mesoporous Al2O3 in a Fluidized Bed Reactor," *Ind Eng Chem Res*, vol. 57, no. 9, pp. 3128–3137, Mar. 2018, doi: 10.1021/ACS.IECR.7B04437/ASSET/IMAGES/MEDIUM/IE-2017-04437X_0007.GIF.
37. A. Li *et al.*, "A novel sludge pyrolysis and biomass gasification integrated method to enhance hydrogen-rich gas generation," *Energy Convers Manag*, vol. 254, p. 115205, Feb. 2022, doi: 10.1016/J.ENCONMAN.2022.115205.
38. F. Salinas and G. García, "Producción de hidrógeno a través de la gasificación de glucosa usando catalizadores de 5%Ni con 2% de La, Ce y Mg y deducción de una ecuación de velocidad de reacción intrínseca," 2019, Accessed: Sep. 12, 2022. [Online]. Available: http://ricaxcan.uaz.edu.mx/jspui/handle/20.500.11845/2306
39. I. Cruz, "Producción de hidrógeno a través de la gasificación de glucosa usando catalizadores de γ-Al2O3 con Ni, Ce y La e interpretación de resultados usando un modelo No-estequiométrico," 2018. Accessed: Sep. 17, 2022. [Online]. Available: https://1library.co/document/y4jjvj9y-produccion-hidrogeno-traves-gasificacion-catalizadores-interpretacion-resultados-estequiometrico.html
40. X. Song and Z. Guo, "Technologies for direct production of flexible H2/CO synthesis gas," *Energy Convers Manag*, vol. 47, no. 5, pp. 560–569, Mar. 2006, doi: 10.1016/J.ENCONMAN.2005.05.012.